https://doi.org/10.5194/egusphere-2025-177
Preprint. Discussion started: 3 March 2025

The Impact of Multi-Scale Turbulence Structures within the Urban Canopy of a Basin City on Haze Pollution Processes

Meiyan Liu [1,3], Yan Ren [1,2], Hongsheng Zhang [4], Min Zhang [5], Jiening Liang [3], Pengfei Tian [3], Xianjie Cao [3], Jiayun Li [3], Lei Zhang [1,3]

[1]Collaborative Innovation Center for Western Ecological Safety, Lanzhou University, Lanzhou 730000, China

[2]Walker Institute, University of Reading, Reading, RG6 6UR, United Kingdom

[3]Key Laboratory for Semi-Arid Climate Change of the Ministry of Education, College of Atmospheric Sciences, Lanzhou University, Lanzhou 730000, China

[4]Laboratory for Climate and Ocean-Atmosphere Studies, Department of Atmospheric and Oceanic Sciences, School of Physics, Peking University, Beijing 100081, China

[5]Donghai Laboratory, Zhoushan 316000, China

Correspondence to: Yan Ren (ry@lzu.edu.cn)

Abstract. The urban canopy layer (UCL) is strongly affected by human activities, with rough elements and anthropogenic heat sources enhancing turbulence complexity. In basin cities, the terrain further complicates the influence of turbulence structures on the haze pollution processes, which still remains unclear. Based on field observations in Lanzhou, China, this study identified a typical evolution pattern of haze pollution in the UCL: $PM_{2.5}$ concentrations rose from 08:00-13:00, declined from 14:00-18:00, rose again from 19:00-21:00, and declined from 22:00-07:00. The occurrence of unexpected thermal plumes promotes the increase in $PM_{2.5}$ concentrations during 10:00-13:00. The rapid removal by small-scale eddies with timescales less than 15 min or even 2 min contributes to the reduction of $PM_{2.5}$ concentrations during 14:00-18:00. At the same time, thermal driven turbulent eddies form organized coherent structures, ejections and sweeps, which affected the exchange of pollutants interior and exterior of the UCL. Turbulence intensity was generally weak, coupled with evening peak emissions leading to a rise in $PM_{2.5}$ concentrations during 19:00-21:00. Finally, sub-mesoscale motions can enhance pollutant dispersion by driving intermittent bursts of turbulence, or reduce pollutant concentrations by forming organized coherent structures during 22:00-07:00. These complex multi-scale atmospheric motions interact and collectively influence the evolution of haze pollution within the basin UCL. These findings are of great significance for understanding the dynamics and thermodynamics of UCL, improving the accuracy of urban air pollution forecasting.

https://doi.org/10.5194/egusphere-2025-177
Preprint. Discussion started: 3 March 2025

1 Introduction

Haze pollution not only severely threatens human health (Cohen et al., 2017), but also has complex impact on weather and climate due to the alteration of atmospheric radiation characteristics by aerosols (Huang et al., 2023). This issue is especially critical in densely populated large-scale urbans, where haze pollution tends to be more severe (Huang et al., 2014). Owing to the unique topography features of basin urbans, adverse atmospheric diffusion conditions are more pronounced (Baker et al., 2011; Lareau et al., 2013), making air pollution control in these areas more complicated than in flatland cities (Baasandorj et al., 2017). Globally, basin cities often experience high-concentration air pollution events during the winter, leading to serious air quality problems (Hallar et al., 2022; Zhao et al., 2023). Research on haze pollution in basin cities are classic and crucial topic, contributing significantly to improving environmental quality and safeguarding human health in many aspects.

The haze pollution processes occur within the atmospheric boundary layer, and its development and dissipation are strongly affected by the structures of atmospheric turbulence. Atmospheric turbulence is the main form of motions in the atmospheric boundary layer, which consists of many vortex structures of different scales. Large-scale coherent vortices can carry more kinetic energy, while small-scale vortices mainly participate in the diffusion of pollutants and the dissipation of energy (Hu, 1998). Atmospheric turbulence determines the extent and height of diffusion of pollutants emitted from the near-surface (Businger et al., 1971). The occurrence of haze pollution is closely related to the stable boundary layer (Stjern et al., 2023). The turbulence intermittency is an inherent characteristic of the stable boundary layer (Allouche et al., 2022), which can be driven by various sub-mesoscale motions. Sub-mesoscale motions refer to non-stationary movements with timescales larger than turbulence motion (Mahrt, 2009). Studies have demonstrated that variations in the intensity of turbulence intermittency significantly influence the accumulation and dissipation of atmospheric pollutants (Wei et al., 2018; Ren et al., 2019). Ren et al. (2021) found that turbulence intermittency can induce the turbulence barrier effect, which hinders the vertical transport of pollutants and results a rapid increase in fine particulate matters. The turbulence barriers can be disrupted by various mechanisms (Sun et al., 2012; Ren et al., 2023), while short-term turbulence bursts can improve vertical diffusion conditions, promoting vertical mixing of pollutants and altering the vertical distribution of aerosols (Wei et al., 2022). Additionally, atmospheric

https://doi.org/10.5194/egusphere-2025-177
Preprint. Discussion started: 3 March 2025

turbulence motions present self-organizing characteristics and self-similarity in both time and space (Katul et al., 1997; Hagelberg and Gamage, 1994), resulting in the formation of coherent structures that significantly influence the transport and diffusion of pollutants (Shi et al., 2022; Jia et al. 2022).

The atmospheric turbulence structures in the urban boundary layer (UCL) are more complex, and their influence on the haze pollution processes is more intricate than that of the natural underlying surfaces. The urban boundary layer consists of the urban near-surface layer and the outer layer (Oke et al., 1987), among which the UCL represents the atmosphere close to the ground layer below the top of urban buildings (Oke et al., 2017). UCL is the most drastically affected by pollution sources emissions from surface and anthropogenic activities. The distribution of rough elements (e.g., buildings, trees) within the UCL is highly inhomogeneous in three-dimensional space, and the development of turbulent eddies can easily be restricted or fragmented by the influence of rough elements. Moreover, the atmospheric stratification within the UCL tends remain an unstable state, even at night, due to the large amount of heat stored in buildings and the additional energy input from anthropogenic activities (Wood et al., 2010; Lietzke and Vogt, 2013; Schmutz et al., 2016). Consequently, atmospheric turbulence within the UCL is characterized by strong non-stationarity and inhomogeneity. These turbulence structures exhibit multi-scale properties (Román-Cascón et al., 2023) that may be influenced by sub-mesoscale motions (Ren et al., 2019). Existing classical theories have limitations when applied to the UCL (Roth., 2000; Zou et al., 2015), and turbulent energy spectra differ significantly from those observed over flat and homogeneous surfaces (Roth et al., 1993). Although the UCL is most closely related to the human production and life, the presence of highly heterogeneous roughness elements and anthropogenic influences complicates the study of atmospheric turbulence structures within the UCL. As a result, the mechanisms by turbulence structures within the UCL affect pollution processes remain poorly understood, significantly hindering the accurate forecasting of urban pollution.

The unique topography of basins more prone to inducing cold pool events that will result in the formation of stable boundary layer (Lareau et al., 2013). However, simultaneously, behaviours such as urban heating increase anthropogenic heat sources and promote the development of an unstable boundary layer. These two opposite processes will result in different atmospheric turbulence structures, influencing haze pollution events distinctly. Therefore, how does the complicated multi-scale turbulent structures within the UCL of basin influence the occurrence and evolution of haze pollution events? This scientific

https://doi.org/10.5194/egusphere-2025-177
Preprint. Discussion started: 3 March 2025

question is of great significance for understanding the development and variation of the urban boundary layer as well as for improving urban air pollution forecasting. This study utilizes the observation data of high precision atmospheric turbulence and high temporal resolution sounding from the Lanzhou atmospheric components monitoring superstation in January 2021 to examine the general characteristics of the haze pollution processes and turbulence structures within the UCL of basin. Using Lanzhou as a case to investigate the influence of the multi-scale turbulence structures on the haze pollution processes in terms of turbulence diffusion, turbulence intermittency, coherence structure of turbulence and sub-mesoscale motions. This manuscript is organized as follows: Section 2 describes the data and methods, Section 3 presents the results, and Section 4 displays the conclusions.

2 Data and methods

2.1 Field Campaign

The observation datasets utilized in this study come from the Lanzhou atmospheric components monitoring superstation (LACMS, 36.05°N, 103.87°E) situated in the Lanzhou Basin (Du et al., 2020). The Lanzhou Basin is located in the narrow Yellow River valley on the northeastern edge of the Tibetan Plateau. The overall topography has a northwest-southeast orientation (Fig. 1a), with an average elevation of 1520 m. The surrounding northern and southern mountains rise 200-600 m above the basin floor. Lanzhou city is situated in the semi-arid region of northwestern China and serves as a major industrial base and a key comprehensive transportation hub. The area around LACMS is primarily composed of academic and residential buildings (Fig. 1b), with a heavy traffic north-south urban trunk road located about 300 m to the west. LACMS stands atop an academic building at Lanzhou University, approximately 38.5 m above the ground. The UCL height is approximately 50 m according to the average height of nearby buildings, and LACMS lies within the UCL. A three-dimensional ultrasonic anemometer (CSAT-3B, Campbell Scientific Inc., USA), sampling at 10 Hz, was installed approximately 2.8 m above the roof to measure wind velocity components and sonic temperature. Hourly $PM_{2.5}$ concentrations (μg m^{-3}) and CO concentrations (mg m^{-3}) were measured by a particulate matter synchronous mixing monitor (5030i SHARP, Thermo Fisher, USA) and an online gas analyzer (48i; Thermo Fisher Scientific, USA), respectively. Hourly relative humidity (RH) was recorded by

https://doi.org/10.5194/egusphere-2025-177
Preprint. Discussion started: 3 March 2025

meteorological sensors (FWE500, FRT, China). The encrypted sounding observations were conducted in January 2021, detailed information of which is described in Zhang et al. (2024). The Vaisala RS41 radiosonde (Vaisala Oyj Inc., Finland) observed the meteorological elements profiles of vertical atmospheric column, including wind speed and temperature. The Micro-Pulse Lidar (MiniMPL, Sigma Space Inc., USA) provided a row standardized backscattered signal at 532 nm. In addition, all data and results in this study are presented at Beijing Standard Time (BJT= UTC + 8 h).

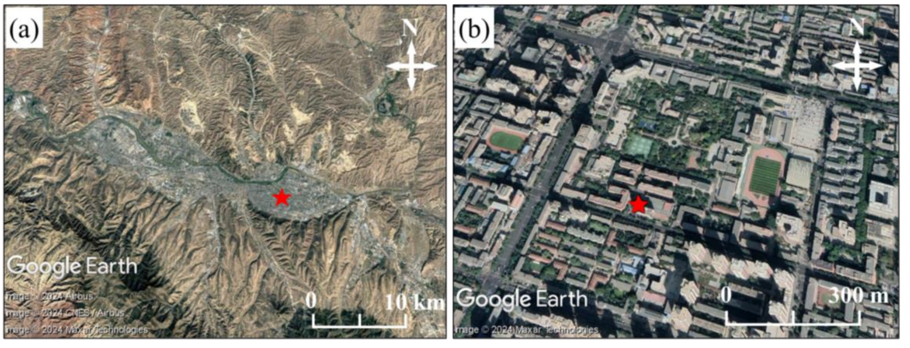

Figure 1. (a) Topographic and geomorphologic map of the Lanzhou Basin obtained from © Google Earth, with the red pentagram as the location of the observing site; (b) Lanzhou atmospheric components monitoring superstation (LACMS) located in the urban underlying surface region marked by the red pentagram (within a range of approximately 1 km)

2.2 Turbulence data preprocessing

The raw turbulence datasets from January 2021 were preprocessed using Eddy Pro software (Advanced mode, V version 6.2.1, LI-COR Biosciences, Inc., USA), and the averaging intervals were set to 30 min to calculate the turbulence statistics. The pre-processing procedures included exceptional point deletion, error flags, quadratic coordinate rotation, and detrending. Then, turbulent statistics, such as turbulent kinetic energy (TKE), friction velocity (u_*), sensible heat flux (H), and the local Obukhov length (L) are calculated as follows:

$$\mathrm{TKE} = \frac{1}{2}\left(\overline{u'^2} + \overline{v'^2} + \overline{w'^2}\right) \tag{1}$$

$$u_* = [(-\overline{u'w'})^2 + (-\overline{v'w'})^2]^{1/4} \tag{2}$$

$$\mathrm{H} = \rho C_P \overline{w'\theta'} \tag{3}$$

https://doi.org/10.5194/egusphere-2025-177
Preprint. Discussion started: 3 March 2025

$$L = -\frac{\bar{\theta} u_*^3}{\kappa g \overline{w'\theta'}} \quad (4)$$

where: u, v and w are along-wind, across-wind and vertical velocity components, respectively; θ is the potential temperature; ρ is the air density; C_p is the specific heat capacity at constant pressure; κ and g are the von Karman constant (0.4) and the gravitational acceleration (9.81 m s^{-2}), respectively. The prime and overbar denote the turbulent fluctuations and Reynolds means, respectively. The local atmospheric stability parameter within the UCL is represented by (z-d)/L, where z is the observed height (approximately 41.3 m), d is the zero-plane displacement (approximately 37.5 m).

2.3 Methodology and indicators

1) Multi-resolution decomposition (MRD)

The Multi-Resolution Decomposition (MRD) method was utilized to analyze multi-scale turbulent eddy characteristics in this study. MRD employs the Haar wavelet basis function to quantify the contribution of turbulent eddies across various time scales to the turbulence variance or covariance (e.g., TKE, u_*, H). This is achieved by decomposing turbulence variances or covariances into different time scales using sliding averaging window (Vickers and Mahrt. 2003; Vickers and Mahrt. 2006; Acevedo et al. 2014).

2) The separation and reconstruction algorithm of sub-mesoscale and turbulent motions (SMT)

In our study, we used the automated algorithm developed by Ren et al. (2019) for the separation and reconstruction of sub-mesoscale and turbulent motions (SMT). The SMT algorithm is based on the Hilbert-Huang transform (HHT). It first uses the complementary ensemble empirical modal decomposition (CEEMD) to transform raw 30 min turbulence data into intrinsic modal functions (IMFs) with different instantaneous frequencies. Subsequently, the algorithm calculates the second-order Hilbert spectra, identifying spectral gaps that separated the small-scale motion (turbulence) and large-scale motion (sub-mesoscale motion). The frequency of spectral gaps is obtained by finding the frequency interval in which the values of the second-order Hilbert spectrum remain almost unchanged. Lastly, all IMFs with frequencies larger than the gap frequencies are added to reconstruct sub-mesoscale motions, while all IMFs with frequencies smaller than the gap frequencies are added to reconstruct the turbulence. The deviations of three-dimensional wind speeds of turbulence (sub-mesoscale motions) are u'_{turb} (u'_{sub}), v'_{turb} (v'_{sub}), and w'_{turb} (w'_{sub}). Ren et al. (2019; 2023) defined the local intermittent strength of turbulence (LIST), the kinetic energy of turbulence motion (KE_{turb}), the kinetic energy of sub-

https://doi.org/10.5194/egusphere-2025-177
Preprint. Discussion started: 3 March 2025

mesoscale motion (KE_{sub}) and the difference in kinetic energy between turbulence and sub-mesoscale motions (ΔKE). LIST reflects the characteristics of dynamics intermittency. According to this definition, smaller LIST values correspond to lower proportion of the turbulent signals in the original pulsation signal, indicating a greater influence of sub-mesoscale motions and stronger turbulence intermittency, and vice versa.

$$KE_{turb} = \frac{1}{2}\left(\overline{{u'_{turb}}^2} + \overline{{v'_{turb}}^2} + \overline{{w'_{turb}}^2}\right) \tag{5}$$

$$KE_{sub} = \frac{1}{2}\left(\overline{{u'_{sub}}^2} + \overline{{v'_{sub}}^2} + \overline{{w'_{sub}}^2}\right) \tag{6}$$

$$LIST = \frac{\sqrt{KE_{turb}}}{\sqrt{KE_{turb}+KE_{sub}}} \tag{7}$$

$$\Delta\mathrm{KE} = KE_{turb} - KE_{sub} \tag{8}$$

Then, the coherence degree of sub-mesoscale motions is represented quantitatively using the correlation coefficient defined by Zeng et al. (2010):

$$R_{sub} = \overline{u'_{sub}w'_{sub}}/(\overline{{u'_{sub}}^2{w'_{sub}}^2})^{1/2} \tag{9}$$

3) Quadrant analysis

The quadrant analysis method was used to study the turbulent coherent structures. The turbulent coherent structures mainly consist of ejections and sweeps (Li and Bou-Zeid, 2011), and different topology of turbulent coherent structures can be identified based on the characteristics of the difference in the flux contribution and time fraction of ejections and sweeps. According to the definition of quadrant analysis (Katul et al., 1997), the vertical velocity fluctuation w' is prescribed as the y-axis, and the horizontal wind velocity fluctuation u' or temperature fluctuation θ' as the x-axis. For momentum fluxes, quadrants 2 and 4 represent ejections and sweeps, respectively, while quadrants 1 and 3 represent outward interactions and inward interactions, respectively. The counter-gradient motions of momentum fluxes by the outward interactions and inward interactions produce upward momentum fluxes (i.e., $\overline{w'u'} > 0$) and weaken the net downward momentum transport. For the sensible heat flux, when $\overline{w'\theta'} > 0$, quadrants 1 and 3 stand for ejections and sweeps, respectively, while when $\overline{w'\theta'} < 0$, quadrants 2 and 4 stand for ejections and sweeps, respectively. Similar to the definition of momentum flux, the other two quadrants correspond to outward interactions and inward interactions, respectively.

https://doi.org/10.5194/egusphere-2025-177
Preprint. Discussion started: 3 March 2025

For a given 30-min interval, the flux contribution $S_{i,wa}$ and the time fraction $T_{i,wa}$ of each quadrant (turbulent motions) are quantified as:

$$S_{i,wa} = \frac{\overline{|w'a'|}_i}{\overline{|w'a'|}} = \frac{\sum_{n=1}^{N} |w'a'|_n I_i(n)}{\sum_{n=1}^{N} |w'a'|_n} \tag{10}$$

$$T_{i,wa} = \frac{\sum_{n=1}^{N} I_i(n)}{N} \tag{11}$$

Where a=u or θ, i is the order of the quadrant (i = 1, 2, 3, 4), N is the total number of records in the 30 min interval, and $I_i(n)$ is an indicator function. If $w'a'$ is located in quadrant i, then $I_i(n)$=1, otherwise $I_i(n)$=0.

Quadrant analysis was applied to obtain the contributions of momentum flux of sub-mesoscale motions in each quadrant, and further calculating the flux contribution difference between downward and upward motions (ΔS), R_{sub} from Eq. (9). A positive ΔS indicates that downward motions predominate.

$$\Delta S = \begin{cases} S_{3,w'_{sub}u'_{sub}} - S_{1,w'_{sub}u'_{sub}} & R_{sub} > 0 \\ S_{4,w'_{sub}u'_{sub}} - S_{2,w'_{sub}u'_{sub}} & R_{sub} < 0 \end{cases} \tag{12}$$

4) Fourier spectral analysis

Fourier spectral analysis can provide micro information about turbulence structure by calculating the variance spectra, covariance spectra, phase spectra and coherence spectra of the variables (Kaimal et al., 1972; Stull, 1988), such as the contribution from turbulent eddies with different scales, phase difference and coherence between the time series of the different variables. Physically, the phase spectra can measure the synchronization of two time series, while the coherence spectra reflect the frequency-dependent correlation coefficient. When the changes in two time series are synchronous, the phase difference would be 0, i.e., minima of one time series concur with minima or maxima of the other. Otherwise, large absolute values of phase difference suggest poor synchronization and the separation between the respective physical processes. The values of coherence spectra in the range of 0 to 1, with larger values indicating better coherence between the two time series at a given frequency.

2.4 Pollution case

According to the second level of National Ambient Air Quality Standards (NAAQS) of China (Ministry of Environmental Protection, 2012), the daily average $PM_{2.5}$ concentrations observed by LACMS exceeded 75 μg m^{-3} on January 2, 12-13, 18, and 20-22, 2021. In this paper, the periods of January 11-14 and 17-21, 2021 were selected as two haze pollution events, referred to Case 1 and Case 2. The clean

https://doi.org/10.5194/egusphere-2025-177
Preprint. Discussion started: 3 March 2025

periods were January 4-10, 15-16, and 24-31, respectively. The highest concentration of $PM_{2.5}$ in Case 1 and Case 2 was 126 μg m^{-3} and the lowest concentration was 21 μg m^{-3}. During this period, Lanzhou experienced the cold winter season, with local emissions from heating boilers, urban transportation, and industrial production being the main sources of pollutants.

3 Results

3.1 Overview of haze pollution processes and turbulent transport within the UCL of basin

The haze pollution processes within the UCL of Lanzhou Basin exhibited distinct diurnal variation characteristics. During the pollution periods, $PM_{2.5}$ concentrations generally rose from 08:00 to13:00, declined between 14:00 and 18:00, rose again from 19:00-21:00, and finally declined again from 22:00-07:00 the next day (Fig. 2a). $PM_{2.5}$ concentrations during the haze and clean periods followed a similar trend from 08:00-18:00. However, during the haze periods, $PM_{2.5}$ concentrations rose again from 19:00 to 20:00, while they continued to decline during the clean periods. Haze pollution processes were influenced by the combined effects of source emissions and meteorological conditions. CO exhibits strong chemical inertness, making its concentrations in the air are strongly controlled by meteorological parameters within a relatively short period. Therefore, it is considered a good tracer. Source emission characteristics can be obtained using the $PM_{2.5}$/CO ratio method, which accounts for the dilution effects of meteorological processes (Liggio et al., 2016; Wang et al., 2018). For Lanzhou Basin, the daily variation of $PM_{2.5}$/CO during the clean and polluted periods was nearly identical, with slightly higher $PM_{2.5}$/CO values calculated during the clean periods compared to the polluted periods (Fig. 2b). This suggested that meteorological conditions might play a crucial role in the occurrence of haze pollution within the UCL of basin. According to the large-scale circulation background and temperature fields at 500 hPa (Figs. S1), Lanzhou Basin was in the control area of westerly latitudinal circulation during haze pollution periods, without obvious trough or ridge activity. Compared with the clean periods, the circulation evolved more slowly during haze pollution periods, with geopotential height contours being relatively sparse and cold air intensity weaker. During the pollution periods, relative humidity and horizontal wind speed were lower (Fig. 2c and Fig. 2e), whereas near-surface temperature was higher (Fig. 2d). Previous studies indicated that higher relative humidity would promote the hygroscopic growth

https://doi.org/10.5194/egusphere-2025-177
Preprint. Discussion started: 3 March 2025

of fine particulate matters (Quan et al., 2011; Chen et al., 2012), while higher near-surface temperature supposed the development of unstable stratification. It seemed difficult to discuss clearly the decisive contribution of these local meteorological conditions to the formation of haze pollution. Therefore, we would continue to study the impact of turbulence in the local UCL.

TKE, u_*, H and (z-d)/L exhibited obvious diurnal variation, with larger absolute values observed from 13:00-18:00 (Fig. 2f-2i). Overall, TKE and u_* were higher during the clean periods compared to the haze pollution periods, while H was larger and atmospheric instability was stronger during the pollution period from 12:00-18:00. Previous researches have generally found that H in the urban boundary layer was smaller and the atmospheric stratification was more stable during the pollution periods, which were unfavorable for pollutant dispersion (Ren et al., 2018; Wang et al., 2020). However, within the UCL of basin, atmospheric stratification was in an unstable state during much of the pollution periods. Which primarily influenced by the release of anthropogenic heat and urban canopy storage heat, with strong buoyancy effects and great vertical transport capacity of H. In summary, compared to the average turbulent state during the clean periods, the dynamic turbulent effect was weaker, while the thermal effect was stronger during the haze pollution periods in the UCL of basin. Both dynamic and thermal turbulence had complied influence on the evolution of haze pollution processes. Next, we would further analyze the specific details of these two pollution cases from the multi-scale turbulence, explore the causes of this pollution pattern in Lanzhou Basin, and how this turbulent transport condition, which was distinguished from most studies, contributed to haze pollution.

https://doi.org/10.5194/egusphere-2025-177
Preprint. Discussion started: 3 March 2025

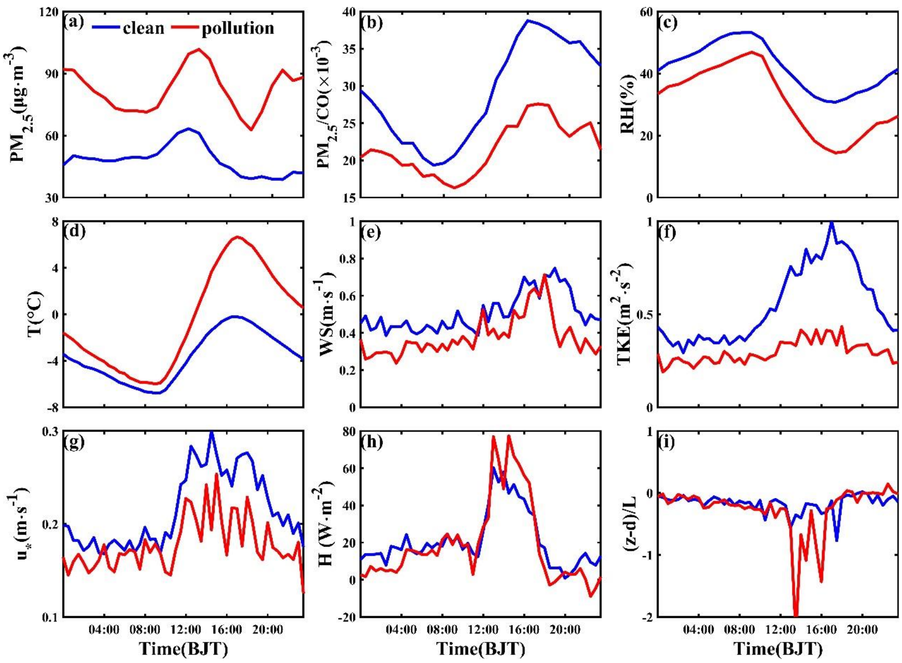

Figure 2. The mean diurnal variation of (a) concentrations of $PM_{2.5}$, (b) $PM_{2.5}$/CO, (c) relative humidity (RH), (d) temperature (T), (e) horizontal wind speed (WS), (f) turbulent kinetic energy (TKE), (g) friction velocity (u_*), (h) sensible heat flux (H), and (i) stability parameter ((z-d)/L) under different conditions from LACMS in January 2021. Solid blue and red lines indicate clean and pollution periods, respectively.

3.2 Influence of small-scale turbulent eddies within the UCL of basin on haze pollution processes

The development of turbulent eddies within the UCL can be easily constrained or fragmented by roughness elements. The contribution of turbulent vortices at different scales to TKE varies. The contribution of turbulent eddies at different scales to TKE during Case 1 and Case 2 was illustrated in Fig. 3. Strong turbulence occurred from 14:00 to 18:00 on January 14, 2021 (red box), with the TKE could reach 3.27 $m^2\ s^{-2}$. While, during the remaining periods, turbulence intensity was weaker, and the TKE did not exceed 1 $m^2\ s^{-2}$. MRD analysis revealed that during the strong turbulence period, the small-scale eddies with timescales shorter than 2 min contributed significantly to TKE, whereas during the weak turbulence period, the large-scale eddies with timescales longer than 15 min generally contributed more to TKE. The periods from 14:00 to 18:00 corresponded to the dissipation phase of $PM_{2.5}$, with larger decreases in $PM_{2.5}$ concentrations on January 14th, 19th, and 21st, 2021. The yellow boxes in Figs.

https://doi.org/10.5194/egusphere-2025-177
Preprint. Discussion started: 3 March 2025

3g and 3i showed that the turbulent eddies with timescales shorter than 15 min from 14:00-18:00 on January 19th and 21st, 2021, contributed significantly to TKE. In summary, the contribution of small-scale turbulent eddies with timescales shorter than 2 min to TKE was greater than that of large-scale eddy eddies with timescales longer than 15 min during the pollution periods. From 14:00-18:00, small-scale eddy eddies with timescales shorter than 15 min or even 2 min can efficiently remove the fine particle matters, resulting in the reduction of $PM_{2.5}$ concentrations.

Acevedo et al. (2014) found that TKE increased exponentially with the time scale in the sub-mesoscale motions range. Fig. 3 showed that when the eddy scale exceeded a certain threshold (e.g., 15 min), the TKE spectral value increased with the timescale. That suggested the presence of sub-mesoscale motions in this situation. In the two pollution cases we analyzed, sub-mesoscale motions were consistently present, and the presence of sub-mesoscale motions could drive the occurrence of turbulent intermittency events (Sun et al., 2012), which significantly influenced the development and evolution of haze pollution under weak turbulence conditions (Ren et al., 2023). Next, we discussed the energy transition process between turbulence and sub-mesoscale motions and its effect on the evolution of $PM_{2.5}$ concentrations during turbulent intermittency events in the UCL of basin through the variation of local intermittent strength of turbulence (LIST), kinetic energy of turbulence and sub-mesoscale motions (KE_{turb} and KE_{sub}), and the difference in energy between them (ΔKE, $\Delta KE = KE_{turb} - KE_{sub}$) over time.

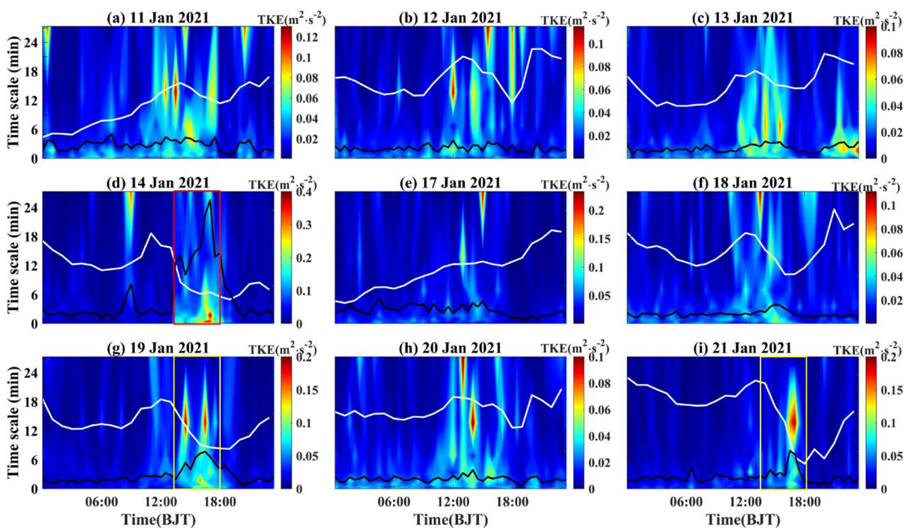

https://doi.org/10.5194/egusphere-2025-177
Preprint. Discussion started: 3 March 2025

Figure 3. Multi-Resolution Decomposition (MRD) spectra of turbulent kinetic energy (TKE) for Case 1 (January 11–14, 2021, a-d) and Case 2 (January 17–21, 2021, e-i) over 30 min time scales. The solid black and white lines represent TKE average values within 30 min and the $PM_{2.5}$ concentrations, respectively, and the filled colour denotes the TKE spectrum values.

From Fig. 4b, 4c, and 4d (yellow arrows), it can be observed that between 08:00 and 13:00, LIST, KE_{turb} and ΔKE were decreasing, while KE_{sub} was increasing. Which suggested that the energy of the small-scale mechanical turbulence was dissipating, the influence of the sub-mesoscale motions was relatively increasing, and the was decreasing gradually. According to the previous MRD analysis, the large-scale turbulent eddies with timescales longer than 15 min were disturbed by the sub-mesoscale motions. During these periods, the dynamical intensity of turbulence intermittency was stronger, coupled with the increase in primary source emission intensity, leading to the $PM_{2.5}$ concentrations gradually rose. Subsequently, at 14:00-18:00 due to the increase in wind speed and buoyancy, wind shear caused by flow through rough elements and buoyancy convection provided the energy sources. Entering the turbulence burst periods, the turbulence effect gradually intensified (red arrow), with the turbulence intensity reaching maximum, resulting in a corresponding decrease in $PM_{2.5}$ concentrations. At 19:00-22:00 the turbulence intensity weakened and ΔKE rapidly decreased or even ΔKE <0 (green arrow in Fig. 4d). Combined with the increase of primary emission, caused $PM_{2.5}$ concentrations rose again.

Ren et al. (2023) indicated that a sharp reduction of kinetic energy of turbulent contributed to the enhancement of the turbulent barrier effect, and the energy transition of sub-mesoscale to turbulent motions triggered the breaking of turbulent barrier. After ΔKE < 0, the turbulent barrier tended to be broken, followed by a significant increase in ΔKE. In the two haze pollution cases analysed in this study, the wind speed threshold of turbulence intensity ($V_{TKE} = \left[(\frac{1}{2})(\sigma_u^2 + \sigma_v^2 + \sigma_w^2)^{1/2}\right]$) was determined as 0.75 m s^{-1} (Fig. S2) according to the method of Sun et al. (2012). At night (19:00-07:00 the next day), the wind speeds were below 0.75 m s^{-1}, and the turbulence intensity was lower, which belonged to regime 1 as Sun et al. (2012) suggested. Intermittency turbulent events were driven by sub-mesoscale motions. At 19:00-22:00 (green arrow in Figure 4d), there was a point where ΔKE < 0, which was quickly followed by a significant increase in ΔKE in the subsequent short period. The phenomenon of energy transfer from sub-mesoscale to turbulence motions occurred, corresponding to the increasing KE_{turb} and

https://doi.org/10.5194/egusphere-2025-177
Preprint. Discussion started: 3 March 2025

decreasing KE_{sub}. Therefore, the horizontal wind speeds and the turbulence intensity at night were lower, while the LIST gradually increased. These short-term turbulent bursts might break the turbulent barrier of the layer and promote the transfer and exchange of substances, which leaded to a decrease in $PM_{2.5}$ concentrations.

During 00:00-07:00 on January 14, 2021, the horizontal wind speeds were lower, LIST, ΔKE and KE_{turb} continuously decreased (blue arrows in Fig. 4b, 4c and 4d). This period was in the turbulent quiescent period with high turbulence intermittency intensity, yet it corresponded to a decrease of $PM_{2.5}$ concentration. The scavenging effect of the sub-mesoscale motions required further attention, which would be discussed in the following sections. Overall, turbulence intermittency within the UCL also significantly affected the development of haze pollution, in agreement with other studies in the near-surface layers of urban (Ren et al., 2019) and relatively flat area (Li et al., 2023).

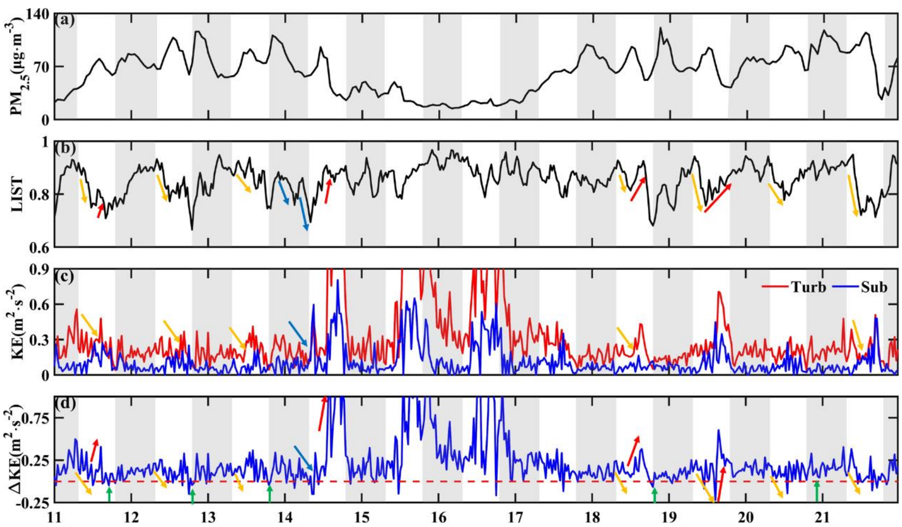

Figure 4. Time series of (a) $PM_{2.5}$ concentration, (b) local intermittent strength of turbulence (LIST), (c) kinetic energy of turbulence (KE_{turb} solid red line) and kinetic energy of sub-mesoscale motion (KE_{sub} solid blue line), and (d) the kinetic energy difference ($\Delta KE = KE_{turb} - KE_{sub}$) from January 11 to 21, 2021. The gray shading represents night between 19:00 and 07:00 the following day.

https://doi.org/10.5194/egusphere-2025-177
Preprint. Discussion started: 3 March 2025

3.3 Influence of large-scale coherent structure within the UCL of basin on haze pollution processes

Although the development of turbulent vortices in UCL was constrained by rough elements, thermal turbulence might still have some coherent structures that affected the transport and diffusion of fine particulate matters. We utilized quadrant analysis to examine the turbulent coherent structures within the UCL of basin on the momentum flux and sensible heat flux transport. The presence of the UCL disrupted the downward transport of momentum, and the release outward from the urban heat storage during the night time likely resulted in a positive sensible heat flux, which are consistent with other studies (Zou et al., 2017; Shi et al., 2019). The downgradient transport of momentum fluxes generally occurred from 14:00-18:00 (shaded gray in Fig. 5c and 5d), with the sweeps (quadrant 4, solid green line) dominating the transport of momentum fluxes, whereas the outward interactions and inward interactions motions (quadrants 1 and 3, solid black and blue lines) dominated the counter-gradient transport of momentum fluxes in most of the other time periods. For the sensible heat flux (Fig. 5e and 5f), during the clean periods (not shown in the figure), the ejections and sweeps (quadrants 1 and 3, black and blue solid lines) dominated throughout most of the day, presenting $\overline{w'\theta'} > 0$. Only occasionally at night or early in the morning, the ejections and sweeps (quadrants 2 and 4, solid red and green lines) dominated or four quadrants contributed equally, presenting $\overline{w'\theta'} < 0$. While during polluted periods, this situation was more common at night or the early morning, because stable boundary layer was more likely to occur at night or early in the morning when there was pollution.

The coherent structures of turbulent flows in UCL contributed significantly to the development of the boundary layer above UCL and the pollutants transport. As shown by the gray shadow in Fig. 5e, 5f, 5g and 5h the flux contributions of ejections (quadrant 1, solid black line) were greater than sweeps (quadrant 3, solid blue line) from 10:00 to 13:00, while the time fraction of ejections (quadrant 1, solid black line) were smaller than sweeps (quadrant 3, solid blue line). That was, less but intense updrafts surrounded by numerous but weak downdrafts, which was well consistent with the behaviour of thermal plumes (Stull, 1988). Maitani and Ohtaki (1987) pointed out that the ejections are more efficient than sweeps in transporting heat under unstable conditions. The presence of thermal plumes during pollution periods was slightly more than during clean periods, which enhanced the transportation efficiency of sensible heat flux. That further explained why the sensible heat flux was greater between 12:00 and 18:00

https://doi.org/10.5194/egusphere-2025-177
Preprint. Discussion started: 3 March 2025

during the pollution periods. In addition, the effective transport of sensible heat flux by the thermal plumes promoted the elevation of the atmospheric boundary layer in the afternoon. As shown in the temperature profiles (Fig. S3a and S3c), the temperature inversion layer weakened or disappeared between 11:00 and 17:00, and the fine particulate matters could further diffuse upward into the atmosphere. It was also evident that the aerosol extinction coefficient was higher at the same height during the pollution period (10:00 to 13:00), with the extinction coefficient profiles showing an "up-convex" shape (Fig. 5a and 5b). In this study, the concentration of fine particulate matters generally decreased with height (Fig. 5a and 5b). At 14:00-18:00, sweeps simultaneously transferred momentum flux and sensible heat flux, and also transported cleaner air from the upper part of the canopy downward to the interior of UCL. During this period, the turbulence intensity in the UCL was high, leading to clean air transported downward mix with the fine particulate matters, thus reducing the $PM_{2.5}$ concentrations in the near-surface. Similarly, it can be seen from Fig. 5a and 5b that the peak value of extinction coefficient profiles gradually decreased during 14:00-18:00. However, the extinction coefficient contour at 14:00-18:00 on January 13, 2021 (white box) showed a peak at 400 m and a break at 200 m above the ground. Further analysis of the wind speed profiles during this period revealed that the wind speeds below 500 m were less than 1 m s^{-1} (Fig. S3b), indicating weak diffusion and limiting the vertical extent of the sweeps effect.

In addition to the coherent structure formed by turbulent motions, sub-mesoscale motions could also exhibit organization and coherence. For instance, Cheng et al. (2007) argued that strong winds are often accompanied by gusts with periods of 3 to 6 min, which are mixtures of low-frequency infrasonic waves and gravity waves, displaying a distinct coherent structure. Essentially, the gust is a form of sub-mesoscale motion that possesses coherence and can form an organized structure. The previous analysis indicated that the turbulent eddies within the UCL were broken and susceptible to the influence of sub-mesoscale motions, which could trigger turbulent intermittency events under the weak turbulent conditions. These sub-mesoscale motions also form organized coherent structures that affect the pollution processes. Analogous to the analysis method for coherent structures in turbulence, Fig. 5i, 5j, 5k and 5l display the correlation coefficient R_{sub} and flux contribution difference ΔS for the sub-mesoscale motions. Sect. 3.2 discussed the analysis of turbulence intermittency from 00:00 to 07:00 on January 14, 2021, where strong turbulence intermittency and weak turbulence intensity were observed, but this period

https://doi.org/10.5194/egusphere-2025-177
Preprint. Discussion started: 3 March 2025

was associated with a decrease in $PM_{2.5}$ concentrations. From Fig. 5i and 5k, R_{sub} and $\Delta S > 0$ (gray shading) during 00:00 to 07:00 on January 14, 2021, indicated that the sub-mesoscale motions in this period were dominated by downward motion (i.e., $w'_{sub} < 0$ and $u'_{sub} < 0$). When $w'_{sub} < 0$ and $u'_{sub} < 0$, the relatively clean air outside the UCL or the upper basin was transported downward, which diluted the fine particle matters in the UCL. As shown in the aerosol extinction coefficient profiles (red arrow in Fig. 5a), the zero-contour line of the extinction coefficient gradually extended to the lower part of basin over time from 00:00 to 07:00 on January 14, 2021. Although the turbulence intermittency was strong and the turbulent diffusion ability was weak at this time, the organized structure formed by the larger-scale sub-mesoscale motions played a positive role in the dissipation of $PM_{2.5}$. In other pollution periods, the coherence of sub-mesoscale motions was also greater than 0 between 23:00 and to 07:00 the next day. Despite weak dynamic turbulence intermittency during this time, these organized sub-mesoscale motions might also have contributed to $PM_{2.5}$ removal. For example, when $w'_{sub} > 0$ and $u'_{sub} > 0$ (gray shadows on January 12th, 18th and 20th, 2021), $PM_{2.5}$ with higher concentration in the UCL was transported upward and subsequently removed more easily with the help of stronger airflow above the canopy, resulting in a decrease in $PM_{2.5}$ concentrations.

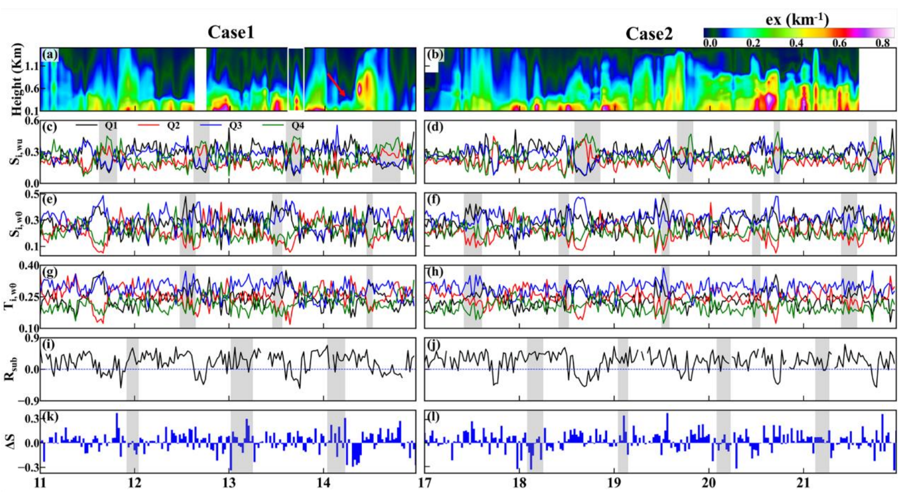

Figure 5. Time series of (a-b) aerosol extinction coefficient profiles, (c-d) flux contribution of each quadrant for momentum, (e-f) flux contribution of each quadrant for sensible heat, (g-h) time fraction of each quadrant for sensible heat flux, (i-j) correlation coefficient of sub-mesoscale motions (R_{sub}), (k-l) flux contribution of sub-mesoscale difference between the downward and upward motion (ΔS) from Case 1 (January 11–14, 2021,

https://doi.org/10.5194/egusphere-2025-177
Preprint. Discussion started: 3 March 2025

left panels) and Case 2 (January 17–21, 2021, right panels). The solid black, red, blue, and green lines represent the results of the quadrants 1, 2, 3, and 4, respectively.

3.4 Characterization of multi-scale turbulence spectra within the UCL of basin at different stages of the pollution processes

The previous analyses have indicated that small-scale turbulent eddy diffusion, intermittency turbulence and coherent structures within the UCL of basin could significantly influence the evolution of pollution processes. Moreover, sub-mesoscale motions could act as a driving factor for generating intermittency turbulence and might also form organized structures that contribute to pollution diffusion. These complex multi-scale atmospheric motions were coupled with each other and affected the evolution of pollution within the UCL of basin. The haze pollution processes within the UCL of basin undergone four typical patterns: the $PM_{2.5}$ concentration rose from 08:00-13:00, decreased from 14:00-18:00, rose again from 19:00-21:00, and decreased once more from 22:00-07:00 the next day. We compared the energy spectra, cospectra, phase spectra and coherence spectra characteristics of these four typical phases to further illustrate the effect of complex multi-scale turbulence structures.

Overall, the energy spectra of u all well follow the -2/3 power law in the inertial subrange. The u spectra (Fig. 6a1-d1) and uw cospectra (Fig. 6a2-d2) revealed a clear spectral gap between sub-mesoscale and turbulent motions. Sub-mesoscale motions, emerging in the frequency range of 10^{-3}~10^{-2} (solid blue line in Fig. 6a1-d1 and 6a2-d2), contributed significantly to both the energy spectra and cospectra. And the peak frequency corresponding to the coherence spectra (Fig. 6a4-d4) with a large value suggested a strong correlation between u' and w', but the absolute value of the phase spectra (Fig. 6a3-d3) was grater than $\pi/16$ indicating that was caused by two different physical processes. This suggested that turbulent and sub-mesoscale motions worked together during the four stages of haze pollution development. The uw cospectra exhibited a peak value in the frequency range of 10^{-1} to 10^{0} (solid black line in Fig. 6b2), reflecting those small-scale mechanical eddies had a great contribution to momentum flux. The uw cospectra corresponding to its peak frequency was low (Fig. 6b4), and the phase spectra (Fig. 6b3) approached 0, indicating small-scale eddies caused changes in u' and w'. Compared with Fig. 6a2-d2, the transport of momentum flux by turbulent motion (solid black line in Fig. 6b2) was greater than transported by sub-mesoscale motions. Sub-mesoscale motions either resulted in

https://doi.org/10.5194/egusphere-2025-177
Preprint. Discussion started: 3 March 2025

counter-gradient transport of momentum flux (integral of covariance spectrum ($f * uw$) was less than 0), or produced a smaller momentum flux (with a lower integral of the covariance spectrum ($f * uw$)). When the sub-mesoscale motion appeared in Fig. 6a, the $PM_{2.5}$ concentration should continue to rise, and Fig. 6b corresponded to the decrease of $PM_{2.5}$ concentration. When the sub-mesoscale motion dominated (solid blue line in Figure 6b1-b4), the corresponding $PM_{2.5}$ dissipation rate was lower. It was testified that the removal efficiency of $PM_{2.5}$ by small-scale turbulence was higher than sub-mesoscale motions from 14:00 to 18:00 during the day.

The turbulent intermittency increased as sub-mesoscale motions became more prominent. From the solid black line in Fig. 6b1 to the solid blue line in Fig. 6c1, the peak frequency of the u spectra shifted from high to low frequencies. Additionally, the coherence spectra and phase spectra corresponding to the peak frequency of the cospectra increased, which suggested that the sub-mesoscale motions and the large-scale turbulent eddies gradually dominated the changes of u' and w' together, with a strong correlation between u' and w'. During this time, the turbulent quiescent periods occurred, and the influence of sub-mesoscale motions was relatively increased. Similarly, the spectra characteristics of turbulence also shifted during the turbulent burst periods. Comparing the solid black line and the solid blue line in Fig. 6d1, the solid blue line bulged upward at low frequencies, indicating the role of sub-mesoscale motions increased with stronger turbulence intermittency. At this point, the peak frequency corresponded to a higher coherence (blue solid line in Fig. 6d4), suggesting that the sub-mesoscale motions were more organized and also contributes positively to the removal of $PM_{2.5}$.

https://doi.org/10.5194/egusphere-2025-177
Preprint. Discussion started: 3 March 2025

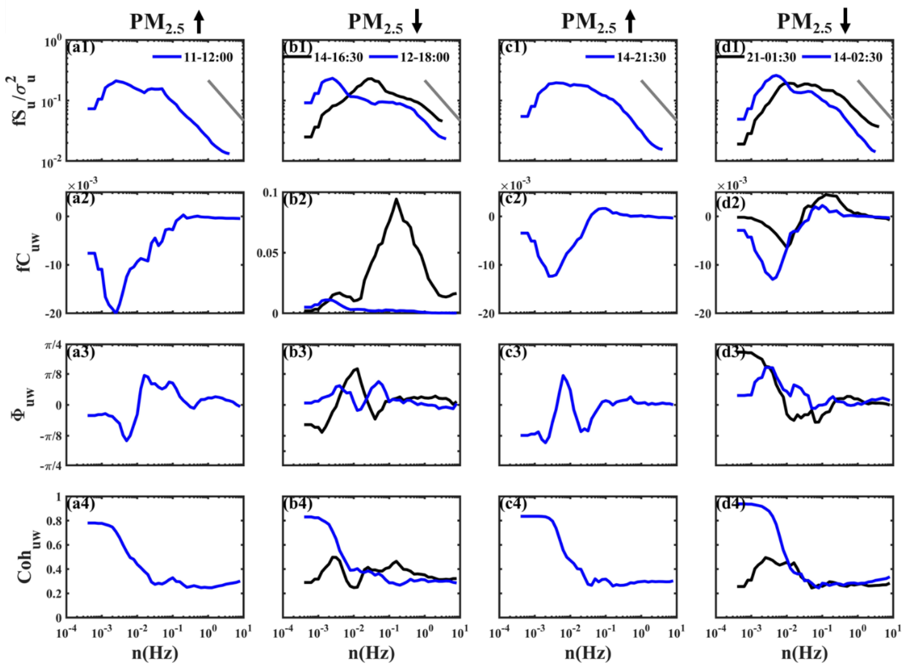

Figure 6. (a1–d1) Energy spectra of u, (a2–d2) covariance spectra of uw, (a3–d3) phase spectra of uw, and (a4–d4) coherence spectra of uw within the UCL of basin. Six time points were selected to represent the following: (a1-a4) 08:00–13:00 on the January 11, 2021, (b1-b4) 16:30 on the January 14, 2021 (solid black line) and 18:00 on the January 12, 2021 (solid blue line); (c1-c4) 21:30 on the on the January 14, 2021, (d1-d4) 01:30 on the on the January 21, 2021 (solid black line) and 02:30 on the January 14, 2021 (solid blue line).

4 Conclusion

The spatial and temporal distribution and variation of fine particulate matters are closely related to atmospheric turbulence motions. Due to the common influence of complicated basin urban underlying surface and anthropogenic heat sources, the turbulence structures within UCL of basin exhibited unique characteristics, and the mechanisms of their influence on the pollution processes were not completely clear. In this study, the general characteristics of the haze pollution processes and turbulence structures within the UCL of the Lanzhou Basin were analyzed by using the turbulence and vertical sounding data from the LACMS in January 2021, and the influence mechanisms of the complex multi-scale turbulence structures within the UCL of basin on the haze pollution processes were further explored. The time series

https://doi.org/10.5194/egusphere-2025-177
Preprint. Discussion started: 3 March 2025

revealed that the haze pollution processes in the UCL of the Lanzhou Basin experienced a typical pattern: the $PM_{2.5}$ concentrations increased from 08:00 to 13:00, decreased from 14:00 to 18:00, increased again from 19:00 to 21:00, and decreased once more from 22:00 to 07:00 the next day. In January of winter, the source emissions were slightly higher during the clean periods than during the pollution periods in Lanzhou, which indicated local meteorological conditions played a critical role in the occurrence of haze pollution processes. The TKE and turbulent fluxes in the UCL of basin exhibited obvious diurnal variation characteristics, which were stronger in the day and weaker at night. Moreover, due to the influence of anthropogenic heat sources, stable stratification occurred only briefly during the pollution processes, while unstable stratification occurred in most cases. The TKE and momentum fluxes in the cleaning periods were greater than in the pollution periods. But the thermal plumes appeared during the pollution periods from 12:00-18:00, which effectively transported the sensible heat flux, making the values larger during the pollution period. These turbulent structural features were different from other natural underlying surfaces.

Next, two haze pollution cases were analyzed in detail to examine the influence of turbulence structures in the UCL on haze pollution evolution, as shown in Fig. 7. The analysis found that the thermal plumes effectively transported sensible heat flux from 10:00 to 13:00, which promoted the elevation of the atmospheric boundary layer in the afternoon, and the $PM_{2.5}$ could further diffuse upward to the upper layer of the atmospheric boundary layer. Between 10:00 and 13:00, small-scale eddies with timescales less than 15 min or even 2 min could efficiently remove fine particulate matters, resulting in a decrease in $PM_{2.5}$ concentrations. The sweeps also could transport the cleaner air from the upper part of the UCL to its inner part. At this time, the high turbulence intensity facilitated the mixing of clean air transported downward and the fine particulate matters, thus reducing the $PM_{2.5}$ concentrations in the near surface layer. From 19:00 to 21:00, the turbulence intensity was weak on the whole, and the effect of turbulence gradually decreased. The emergence of the evening peak resulted in a rapid increase in primary emissions, leading to increase again in $PM_{2.5}$ concentrations. From 22:00 to 07:00 the following day, the intensity of turbulence in the UCL remained still weak. However, when intermittency turbulence events driven by sub-mesoscale motions occurred, short-term intermittency turbulence reduced $PM_{2.5}$ concentrations. In addition, we found that the sub-mesoscale motions could also form certain organized coherent structures, which might play a positive role in the dissipation of $PM_{2.5}$ concentrations. Finally, by comparing the

https://doi.org/10.5194/egusphere-2025-177
Preprint. Discussion started: 3 March 2025

characteristics of energy spectra, cospectra, phase spectra and coherence spectra of the four typical haze pollution stages, this study further confirmed the complex multi-scale effects of turbulence and sub-mesoscale motions within the UCL of basin during different pollution phases.

The results of this study demonstrated that the atmospheric turbulence structure of the UCL in the basin is highly complicated due to the influence of the heterogeneous distribution of rough elements and human activities. Although turbulent eddies developed at small scales, they played a significant role in the diffusive removal of pollutants. Thermal driven turbulent eddies might form organized coherent structures, such as ejections (thermal plumes) and sweeps, which affected the exchange of pollutants interior and exterior the UCL. Moreover, under the influence of heterogeneous surfaces, sub-mesoscale motions also played a significant role. Which could contribute to driving intermittency turbulence and might form coherent structures with certain organization to participate in pollution diffusion. These complex multi-scale atmospheric motions interacted and jointly impacted the evolution of pollution within the UCL of basin. The results of this study are crucial for the improvement of urban air pollution forecasting capabilities.

https://doi.org/10.5194/egusphere-2025-177
Preprint. Discussion started: 3 March 2025

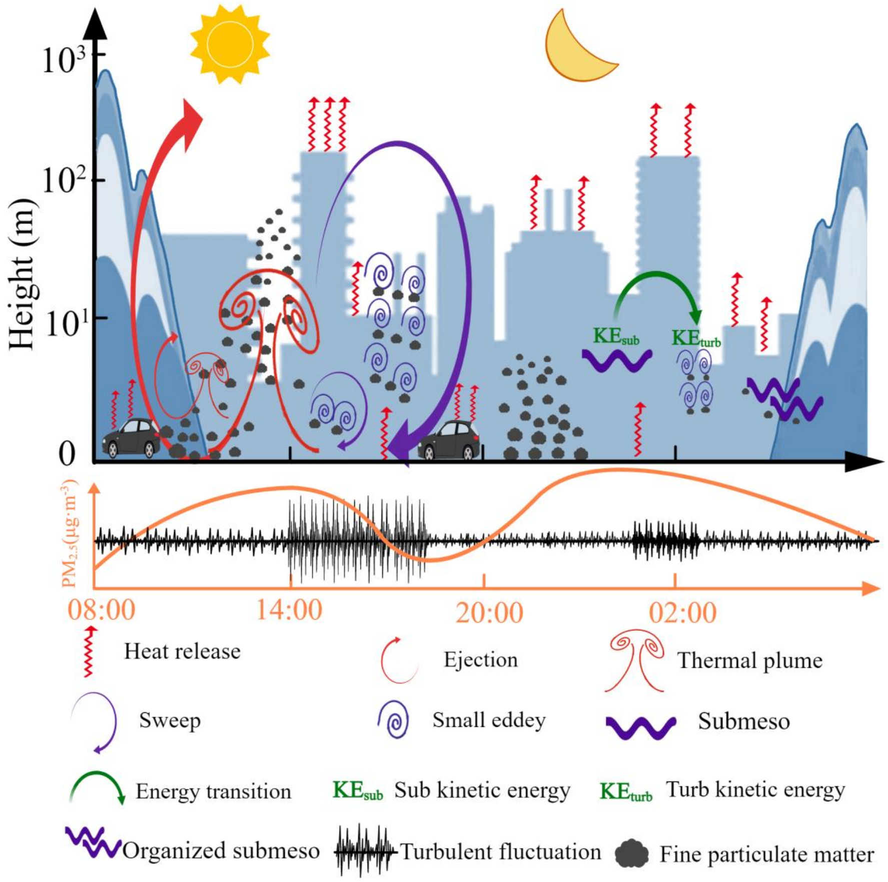

Figure 7. General characteristics of the turbulence structures within the UCL of basin and a schematic diagram illustrating the influence mechanism of the multi-scale turbulence structures on the haze pollution processes.

Code Data availability. Data will be made available on request.

Author contributions. Yan Ren determined the goal of this study. Meiyan Liu carried this out. Meiyan Liu wrote the manuscript draft with the help of Yan Ren and Hongsheng Zhang. Min Zhang helped to process sounding data. Lei Zhang, Hongsheng Zhang and Yan Ren designed the field experiment, Min Zhang, Jiening Liang, Pengfei Tian, Xianjie Cao and Jiayun Li carried the field experiment out and got the data. All authors reviewed and edited the manuscript.

https://doi.org/10.5194/egusphere-2025-177
Preprint. Discussion started: 3 March 2025

Competing interests. The authors declare no competing interests.

Acknowledgement. This work was jointly funded by grant the National Key Research and Development Program of China (2023YFC3708202, 2023YFC3706300), National Natural Science Foundation of China (42475184, 42305071, 42175092), Natural Science Foundation of Gansu Province (23JRRA1045)，Lanzhou Youth Science and Technology Talent Innovation Project(2023-QN-24) and Longyuan Youth Talent Project.

References

Acevedo, O. C., Costa, F. D., Oliveira, P. E. S., Puhales, F. S., Degrazia, G. A., and Roberti, D. R.: The influence of submeso processes on stable boundary layer similarity relationships, J. Atmos. Sci., 71, 207–225, https://doi.org/10.1175/JAS-D-130131.1, 2014.

Allouche, M., Bou-Zeid, E., Ansorge, C., Katul, G. G., Chamecki, M., Acevedo, O., Thanekar, S., and Fuentes, J. D.: The detection, genesis, and modeling of turbulence intermittency in the stable atmospheric surface layer, J. Atmos. Sci., 79, 1171–1190, https://doi.org/10.1175/JAS-D-21-0053.1, 2022.

Baasandorj, M., Hoch, S. W., Bares, R., Lin, J. C., Brown, S. S., Millet, D. B., Martin, R., Kelly, K., Zarzana, K. J., Whiteman, C. D., Dube, W. P., Tonnesen, G., Jaramillo, I. C., and Sohl, J.: Coupling between chemical and meteorological processes under persistent cold-air pool conditions: evolution of wintertime $PM_{2.5}$ pollution events and N_2O_5 observations in Utah's Salt Lake Valley, Environ. Sci. Technol., 51, 5941–5950, https://doi.org/10.1021/acs. est.6b06603, 2017.

Businger, J. A., Wyngaard, J. C., Izumi, Y., and Bradley, E. F.: Flux-profile relationships in the atmospheric surface layer, J. Atmos. Sci., 28, 181–189, https://doi.org/10.1175/1520-0469(1971)028<0181:FPRITA>2.0.CO;2, 1971.

Chen, J., Zhao, C. S., Ma, N., Liu, P. F., Göbel, T., Hallbauer, E., Deng, Z. Z., Ran, L., Xu, W. Y., Liang, Z., Liu, H. J., Yan, P., Zhou, X. J., and Wiedensohler, A.: A parameterization of low visibilities for hazy days in the North China Plain, Atmos. Chem. Phys., 12, 4935–4950, https://doi.org/10.5194/acp-12-4935-2012, 2012.

Cheng, X. L., Zeng, Q. C., Hu, F., and Peng, Z.: Gustiness and coherent structure of strong wind in the atmospheric boundary layer (in Chinese), Climatic and Environmental Research, 12, 227–243, 2007.

Cohen, A. J., Brauer, M., Burnett, R., Anderson, H. R., Frostad, J., Estep, K., Balakrishnan, K., Brunekreef, B., Dandona, L., Dandona, R., Feigin, V., Freedman, G., Hubbell, B., Jobling, A., Kan, H., Knibbs, L., Liu, Y., Martin, R., Morawska, L., Pope, C. A., Shin, H., Straif, K., Shaddick, G., Thomas, M., van Dingenen, R., van Donkelaar, A., Vos, T., Murray, C. J. L., and Forouzanfar, M. H.: Estimates and 25-year trends of the global burden of disease attributable to ambient air pollution: an analysis of data from the Global Burden of Diseases Study 2015, Lancet., 389, 1907–1918, https://doi.org/10.1016/S0140-6736(17)30505-6, 2017.

Du, T., Wang, M., Guan, X., Zhang, M., Zeng, H. Y., Chang, Y., Zhang, L., Tian, P. F., Shi, J. S., and Tang, C. G.: Characteristics and formation mechanisms of winter particulate pollution in Lanzhou, Northwest China, J. Geophys. Res-Atmos., 125, e2020JD033369, https://doi.org/10.1029/2020JD033369, 2020.

Hagelberg, C. R., and Gamage, N. K. K.: Structure-preserving wavelet decompositions of intermittent turbulence, Bound-Lay. Meteorol., 70, 217–246, https://doi.org/10.1007/BF00709120, 1994.

Hallar, A. G., Brown, S. S., Crosman, E., Barsanti, K. C., Cappa, C. D., Faloona, I., Fast, J., Holmes, H. A., Horel, J., Lin, J., Middlebrook, A., Mitchell, L., Murphy, J., Womack, C. C., Aneja, V., Baasandorj, M., Bahreini, R., Banta, R., Bray, C., Brewer, A., Caulton, D., de Gouw, J., De Wekker, S. F., Farmer, D. K., Gaston, C. J., Hoch, S., Hopkins, F., Karle, N. N., Kelly, J. T., Kelly, K., Lareau, N., Lu, K., Mauldin, R. L., III, Mallia, D. V., Martin, R., Mendoza, D. L., Oldroyd, H. J., Pichugina, Y., Pratt, K. A., Saide, P. E., Silva, P. J., Simpson, W., Stephens, B. B., Stutz, J., and Sullivan, A.: Coupled air quality and boundary-layer meteorology in western U.S. basins during winter: design and rationale for a comprehensive study, B. Am. Meteorol. Soc., 102, E2012–E2033, https://doi.org/10.1175/BAMS-D-20-0017.1, 2021.

Huang, R. J., Zhang, Y. L., Bozzetti, C., Ho, K. F., Cao, J, J., Han, Y. M., Daellenbach, K. R., Slowik, J. G., Platt, S. M., Canonaco, F., Zotter, P., Wolf, R., Pieber, S. M., Bruns, E. A., Crippa, M., Ciarelli, G., Piazzalunga, A., Schwikowski, M., Abbaszade, G., Schnelle-Kreis, J., Zimmermann, R., An, Z., Szidat, S., Baltensperger, U., Haddad, I. E., and Prévôt, A. H.: High secondary aerosol contribution to particulate pollution during haze events in China, Nature, 514, 218–222, https://doi.org/10.1038/nature13774, 2014.

Huang, X., Ding, K., Liu, J. Y., Wang, Z. L., Tang, R., Xue, L., Wang, H. K., Zhang, Q., Tan, Z. M., Fu, C. B., Davis, S. J., Andreae, M. O., and Ding, A. J.: Smoke-weather interaction affects extreme wildfires in diverse coastal regions, Science, 379, 457–461, https://doi.org/10.1126/science.add9843, 2023.

Hu, F.: Atmospheric boundary layer eddy structure identification by orthonormal wavelet expansion (in Chinese), Climatic and Environmental Research, 02, 2–10, 1998.

Jia, W. X., Zhang, X. Y., Zhang, H. S., and Ren, Y.: Turbulent transport dissimilarities of particles, momentum, and heat, Environ. Res., 211, 113111, https://doi.org/10.1016/j.envres.2022.113111, 2022.

Kaimal, J. C., Wyngaard, J. C., Izumi, Y., and Coté, O. R.: Spectral characteristics of surface-layer turbulence, Q. J. Roy. Meteor. Soc., 98, 563–589, https:// doi.org/10.1002/qj.49709841707, 1972.

Katul, G., Kuhn, G., Schieldge, J., and Hsieh, C. I.: The ejection-sweep character of scalar fluxes in the unstable surface layer, Bound-Lay. Meteorol., 83, 1–26, https://doi.org/10.1023/A:1000293516830, 1997.

Lareau, N. P., Crosman, E., Whiteman, C. D., Horel, J. D., Hoch, S. W., Brown, W. O. J., and Horst, T. W.: The persistent cold-air pool study, B. Am. Meteorol. Soc., 94, 51–63, https://doi.org/10.1175/BAMS-D-11-00255.1, 2013.

Li, D., and Bou-Zeid, E.: Coherent structures and the dissimilarity of turbulent transport of momentum and scalars in the unstable atmospheric surface layer, Bound-Lay. Meteorol., 140: 243–262, https://doi.org/10.1007/s10546-011-9613-5, 2011.

Li, Q. H., Zhang, H. S., Zhang, X. Y., Cai, X. H., Jin, X. P., Zhang, L., Song, Y., Kang, L., Hu, F., and Zhu, T.: COATS: comprehensive observation on the atmospheric boundary layer three-dimensional structure during haze pollution in the North China Plain, Sci. China. Earth. Sci., 66, 939–958, https://doi.org/10.1007/s11430-022-1092-y, 2023.

Lietzke, B., and Vogt, R.: Variability of CO_2 concentrations and fluxes in and above an urban street canyon, Atmos. Environ., 74, 60–72, https://doi.org/10.1016/j.atmosenv.2013.03.030, 2013.

Liggio, J., Li, S. M., Hayden, K., Taha, Y. M., Stroud, C., Darlington, A., Drollette, B. D., Gordon, M., Lee, P., Liu, P., Leithead, A., Moussa, S. G., Wang, D., O'Brien, J., Mittermeier, R. L., Brook, J. R., Lu, G., Staebler, R. M., Han, Y. M., Tokarek, T. W., Osthoff, H. D., Makar, P. A., Zhang, J. H., Plata, D. L., and Gentner, D. R.: Oil sands operations as a large source of secondary organic aerosols, Nature, 534, 91–94, https://doi.org/10.1038/nature17646, 2016.

Mahrt, L.: Characteristics of submeso winds in the stable boundary layer, Bound-Lay. Meteorol., 130, 1–14, https://doi.org/10.1007/s10546-008-9336-4, 2009.

Maitani, T., and Ohtaki, E.: Turbulent transport processes of momentum and sensible heat in the surface layer over a paddy field, Bound-Lay. Meteorol., 40, 283–293, https://doi.org/10.1007/BF00117452, 1987.

Ministry of Environmental Protection, Ambient Air Quality Standards (GB 3095-2012) 655, http://www.wxbh.gov.cn/doc/2021/11/04/3479116.shtml, 2012.

Oke, T. R.: Boundary Layer Climates (2nd ed.), Routledge, London, https://doi.org/10.4324/9780203407219, 1987.

Oke, T. R., Mills, G., Christen, A., and Voogt, J. A.: Urban Climates, Cambridge University Press, 525 pp, https://doi.org/10.1017/9781139016476, 2017.

Quan, J., Zhang, Q., He, H., Liu, J., Huang, M., and Jin, H.: Analysis of the formation of fog and haze in North China Plain (NCP), Atmos. Chem. Phys., 11, 8205–8214, https://doi.org/10.5194/acp-11-8205-2011, 2011.

Ren, Y., Zheng, S. W., Wei, W., Wu, B. G., Zhang, H. S., Cai, X. H., and Song, Y.: Characteristics of turbulent transfer during episodes of heavy haze pollution in Beijing in winter 2016/17, J. Meteorol. Res-Prc., 32, 69–80, https://doi.org/10.1007/s13351-018-7072-3, 2018.

Ren, Y., Zhang, H. S., Wei, W., Wu, B. G., Cai, X. H., and Song, Y.: Effects of turbulence structure and urbanization on the heavy haze pollution process, Atmos. Chem. Phys., 19, 1041–1057, https://doi.org/10.5194/acp-19-1041-2019, 2019.

Ren, Y., Zhang, H. S., Zhang, X. Y., Wei, W., Li, Q. H., Wu, B. G., Cai, X. H., Song, Y., Kang, L., and Zhu, T.: Turbulence barrier effect during heavy haze pollution events, Sci. Total. Environ., 753, 142286, https://doi.org/10.1016/j.scitotenv.2020.142286, 2021.

Ren, Y., Zhang, H. S., Wu B. G., Zhang, L., Liang, J. N., and Zhang, X. Y.: Energy transition in the enhancement and break of turbulence barrier during heavy haze pollution, Environ. Pollut., 317, 120770, https://doi.org/10.1016/j.envpol.2022.120770, 2023.

Román-Cascón, C., Yagüe, C., Ortiz-Corral, P., Serrano, E., Sánchez, B., Sastre, M., Maqueda, G., Alonso-Blanco, E., Artiñano, B., Gómez-Moreno, F. J., Diaz-Ramiro, E., Fernández, J., Martilli, A., García, A. M., Núñez, A., Cordero, J. M., Narros, A., and Borge, R.: Wind and turbulence relationship with NO_2 in an urban environment: a fine-scale observational analysis, Urban. Climate, 51, 101663, https://doi.org/10.1016/j.uclim.2023.101663, 2023.

Schmutz. M., Vogt. R., Feigenwinter. C., and Parlow. E.: Ten years of eddy covariance measurements in Basel, Switzerland: seasonal and interannual variabilities of urban CO_2 mole fraction and flux, J. Geophys. Res-Atmos., 121, 8649–8667, https://doi.org/10.1002/2016JD025063, 2016.

Shi, Y., Hu, F., Fan, G. Q., and Zhang. Z.: Multiple technical observations of the atmospheric boundary layer structure of a red-alert haze episode in Beijing, Atmos. Meas. Tech., 12, 4887–4901, https://doi.org/10.5194/amt-12- 4887-2019, 2019.

Shi, Y., Zeng, Q. C., Liu, L., Cheng, X. L., and Hu, F.: Important role of turbulent wind gust and its coherent structure in the rapid removal of urban air pollution, Environmental. Research. Communications., 4, 075001, https://doi.org/10.1088/2515-7620/ac7c5f, 2022.

Stjern, C. W., Hodnebrog, Ø., Myhre, G., and Pisso, I.: The turbulent future brings a breath of fresh air., Nat. Commun., 14, 3735, https://doi.org/10.1038/s41467-023-39298-4, 2023.

Roth, M.: Review of atmospheric turbulence over cities, Q. J. Roy. Meteor. Soc., 126, 941–990, https://doi.org/10.1002/qj.49712656409, 2000.

Roth, M., and Oke, T. R.: Turbulent transfer relationships over an urban surface. I. Spectral characteristics, Q. J. Roy. Meteor. Soc., 119, 1071–1104, https://doi.org/10.1002/qj.49711951311, 1993.

Stull, R. B.: An Introduction to Boundary Layer Meteorology. Springer, 670 pp, https://doi.org/10.1007/978-94-009-3027-8, 1988.

Sun, J. L., Mahrt, L., Banta, R. M., and Pichugina, Y. L.: Turbulence regimes and turbulence intermittency in the stable boundary layer during CASES-99, J. Atmos. Sci., 69, 338–351, https://doi.org/10.1175/JAS-D-11-082.1, 2012.

Vickers, D., and L. Mahrt.: The cospectral gap and turbulent flux calculations, J. Atmos. Ocean. Tech., 20, 660–672, https://doi.org/10.1175/1520-0426(2003)20<660:TCGATF>2.0.CO;2, 2003.

Vickers, D., and Mahrt, L.: A solution for flux contamination by mesoscale motions with very weak turbulence, Bound-Lay. Meteorol., 118, 431–447, https://doi.org/10.1007/s10546-005-9003-y, 2006.

Wang, H. B., Tian, M., Chen, Y., Shi, G. M., Liu, Y., Yang, F. M., Zhang, L. M., Deng, L. Q., Yu, J. Y., Peng, C., and Cao, X. Y.: Seasonal characteristics, formation mechanisms and source origins of $PM_{2.5}$ in two megacities in Sichuan Basin, China, Atmos. Chem. Phys., 18, 865–881, https://doi.org/10.5194/acp-18-865-2018, 2018.

Wang, L. L., Fan, S. H., Hu, F., Miao, S. G., Yang, A. Q., Li, Y. B., Liu, J. K., Liu, C. W., Chen, S. S., Ho, H. C., Duan Z. X., Gao, Z. Q., and Yang, Y. J.: Vertical gradient variations in radiation budget and heat fluxes in the urban boundary layer: a comparison study between polluted and clean air episodes in Beijing during winter, J. Geophys. Res-Atmos., 125, e2020JD032478, https://doi.org/ 10.1029/2020JD032478, 2020.

Wei, W., Zhang, H. S, Wu, B. G., Huang, Y. X., Cai, X. H., Song, Y., and Li, J. D.: Intermittent turbulence contributes to vertical dispersion of $PM_{2.5}$ in the North China Plain: cases from Tianjin, Atmos. Chem. Phys., 18, 12953–12967, https://doi.org/10.5194/acp-18-12953-2018, 2018.

Wei, Z. R., Zhang, H. S., Wei, W., Zhang, X. Y., Cai, X. H., Song, Y., and Zhu, T.: Mechanism of the effect of vertically propagating internal gravity waves on turbulence barrier and pollutant diffusion during heavy haze episodes, Sci. Total. Environ., 845, 157349, https://doi.org/10.1016/j.scitotenv.2022.157349, 2022.

Wood, C, R., Lacser, A., Barlow, J. F., Padhra, A., Belcher, S. E., Nemitz, E., Helfter, C., Famulari, D., and Grimmond, C. S. B.: Turbulent flow at 190 m height above London during 2006–2008: a climatology and the applicability of similarity theory, Bound-Lay. Meteorol., 137, 77–96, https://doi.org/10.1007/s10546-010-9516-x, 2010.

Zeng, Q. C., Cheng, X. L., Hu, F., and Peng, Z.: Gustiness and coherent structure of strong winds and their role in dust emission and entrainment, Adv. Atmos. Sci., 27, 1–13, https://doi.org/10.1007/s00376-009-8207-3, 2010.

Zhao, S. P., He, J. J., Dong, L. X., Qi, S. F., Yin, D. Y., Chen, J. B., and Yu, Y.: Contrasting vertical circulation between severe and light air pollution inside a deep basin: results from the Collaborative Experiment of 3D Boundary-Layer Meteorology and Pollution at the Sichuan Basin (BLMP-SCB), B. Am. Meteorol. Soc., 104, E411–E434, https://doi.org/10.1175/BAMS-D-22-0150.1, 2023.

Zhang, M., Tian, P. F., Zhao, Y. Y., Song, X., Liang, J. N., Li, J. Y., Zhang, Z. D., Guan, X., Cao, X. J., Ren, Y., Shi, J. S., and Zhang, L.: Impact of aerosol-boundary layer interactions on $PM_{2.5}$ pollution during cold air pool events in a semi-arid urban basin, Sci. Total. Environ., 922, 171225, https://doi.org/10.1016/j.scitotenv.2024.171225, 2024.

Zou, J., Zhou, B. W., and Sun, J. N.: Impact of eddy characteristics on turbulent heat and momentum fluxes in the urban roughness sublayer, Bound-Lay. Meteorol., 164, 39–62, https://doi.org/10.1007/s10546-017-0244-3, 2017.

Zou, J., Liu, G., Sun, J. N., Zhang, H. S., and Yuan, R. M.: The momentum flux-gradient relations derived from field measurements in the urban roughness sublayer in three cities in China, J. Geophys. Res-Atmos., 120, 10797–10809, https://doi.org/10.1002/2015jd023909, 2015.